Polymer Bulletin (2021) 78:2765–2790
https://doi.org/10.1007/s00289-020-03235-y

ORIGINAL PAPER

Role of the chemical modification of titanium dioxide surface on the interaction with silver nanoparticles and the capability to enhance antimicrobial properties of poly(lactic acid) composites

M. G. Peña-Juárez, et al. ***[full author details at the end of the article]***

Received: 28 February 2020 / Revised: 11 May 2020 / Accepted: 20 May 2020 / Published online: 29 May 2020

Abstract

In this work, the antimicrobial activity of neat and silanized titanium dioxide deposited with silver nanoparticles was evaluated when it was used as filler in a poly(lactic acid) matrix. The silanization and deposition processes were evaluated by scanning transmission electron microscopy and X-ray photoelectron spectroscopy confirming the chemical modification on the titanium dioxide surface by 3-aminopropyltriethoxy silane and the formation of silver nanoparticles. According to the elemental analysis conducted by energy-dispersive X-ray spectroscopy, more silver, 7.4% higher, was deposited on the oxide when this was previously silanized and when 30% w/w of silver nitrate was used as a precursor. The antimicrobial effect was confirmed for the nanoparticles through the disk diffusion method and for the composites by drop test, against *Staphylococcus aureus* and *Escherichia coli* bacteria; the results showed that the inhibition rate increased by 14.2% and 39.1% for nanoparticles and by 57.6% and 38.8% for composites against each bacteria, respectively, when deposition was performed on silanized titanium dioxide. Also, better mechanical properties were obtained in the composites filled with silanized oxide; the best results were obtained in the PLA/sTiO_2–Ag 20% system with an improvement of 45.7% in tensile stress and of 38.73% for Young's modulus. Finally, the toxicity of the composites was evaluated by seeding peripheral blood mononuclear cells; results show evidence that composites filled with these nanoparticles are non-toxic since these do not migrate from the polymeric matrix, which helps to enhance the prolonged surface antibacterial effect and to open a broad perspective of the commercial use of these composites.

Keywords Antimicrobial activity · Silver nanoparticles · Titanium dioxide · Poly(lactic acid) · Polymer composites

Introduction

Poly(lactic acid) (PLA) has increased interest in recent years due to its wide range of applications in the medical, food, and packaging field [1]. PLA is a well-known biodegradable and biocompatible polymer [2], widely considered as a suitable candidate to replace synthetic polymers due to its, thermal stability, high transparency, biocompatibility, ease of processability, lower environmental impact and reasonable price [3, 4]. In recent years, the necessity for both degradable and antimicrobial materials has been increased due to the priority to reduce residues and environmental pollution. Although PLA exhibits essential characteristics, it presents significant disadvantages as its low performance and functionality due to bacterial attack, which limits its use in major industries such as food packaging, preservation, and agriculture.

To open a broad perspective of PLA to more industrial applications, researches have worked to incorporate fillers, which allow improving the antimicrobial and mechanical properties of the film. The fillers that have been shown better microbicidal properties are silver, copper, zinc, titanium, and iron oxides [5, 6]. Silver has been recognized as an effective antimicrobial agent that exhibits low toxicity in humans [7]. Some industrial, biotechnological, and medical applications of silver, against *Escherichia coli* and *Staphylococcus aureus*, are the use of nanoparticles embedded in copolymers [8], in structural control of materials interfaces, and in health care and food packaging fields [9]. It is well known that the antibacterial activity of silver is due to Ag^+ ions, which interact with the three main components of the bacterial cell: the peptidoglycan cell wall and plasma membrane, bacterial DNA, and bacterial protein, particularly enzymes.

Recently, it is known that silver nanoparticles (AgNPs) also possess considerable antimicrobial activity [10, 11], and it is widely believed that AgNPs bind strongly to thiol groups present in the bacterial cell membrane, thereby breaking down the cell wall and, therefore, destroying the cell; these are also incorporated into the cell membrane, which causes the leakage of intracellular substances and then cell death; and finally, AgNPs also manage to penetrate the cells [10–12]. Nevertheless, AgNPs with diameters below 200 nm tend to aggregate spontaneously, and their stability in the air, water, or sunlight is not good enough for long-term applications, which will decrease their antibacterial performance [13, 14]. To solve this problem, a wide range of metal oxides such as TiO_2, SiO_2, and Al_2O_3 have been used to support AgNPs; therefore, Ag-deposited materials can be homogeneously formed without aggregation [10–17].

TiO_2 has been proven to be the most suitable for widespread environmental applications thanks to non-toxicity, low cost, and excellent degradation of organic pollutants [12, 13, 18]. TiO_2 has called interest in many industrial fields since it is a light-sensitive type n semiconductor that absorbs electromagnetic radiation; it is also a very chemically stable amphoteric oxide, which makes it the most used photocatalyst to degrade organic molecules, as well as to fill polymeric matrices [12, 19, 20]. Furthermore, it is well known that TiO_2 can provide a new tool for the prevention of bacterial contamination and disinfection [21, 22].

Nevertheless, TiO_2 particles tend to agglomerate and precipitate, causing a high density that limits its stability in suspension. In order to avoid this problem, these particles are modified on their surface with the purpose of making them suitable for applications; these modifications improve interactions among materials [20, 23, 24]. TiO_2 particles coated with silane, named silanization process, presents a great option because it allows the surface of metal oxides to be modified, changing their attractive interaction and helping to reduce the problem of agglomeration, reducing its interaction and dispersing very well [19, 20, 25, 26]. Organosilanes have a functional group based on hydrolytically active silicon; their carbon–silicon bond is very stable and nonpolar, and in the presence of an alkyl group, results in low surface energy and hydrophobic effects [19, 20, 25]. These coupling agents are widely used in industry to improve the performance of polymers, the resistance of the compounds to water attack significantly, and have other applications such as treatment of fillers to increase reinforcement and adhesion [19].

In order to improve mechanical properties, PLA could be filled with metal oxides, as titanium oxide, and with nanoparticles (AgNPs) [10, 13, 14, 27]. Studies of silver/polylactide nanocomposites confirm a uniform distribution due to different chemical structures and silver–polymer interactions. This is attributed to a strong interaction between AgNPs and PLA chains, which promoted phase separation of polymer that prevents AgNPs agglomeration in the reduction process [28]. According to the literature [29], it is widely demonstrated that interactions between PLA chain molecules and AgNPs are due to the presence of van der Waals interactions between the hydroxyl groups of PLA and the partial positive charge on the surface of AgNPs.

Various works have been performed to improve the antimicrobial activities of PLA. De Silva et al. [30] prepared films with nanoparticles of ZnO deposited on the surface of halloysite nanotubes (Hal) using a novel solvothermal method; nevertheless, although this filler exhibited promising antimicrobial properties, large amounts of filler (5% and 10%) were required to obtain good results, while several regulations allow only 1% as an additive for the food industry, plus the high costs due to expensive NPs and process prices. On the other hand, Li et al. [9] used a blend of nano-TiO_2 and a silver solution; despite having good inhibition results, the method presented two main problems, the first is that these types of fillers had problems of miscibility and interfacial interaction in TiO_2 and PLA; therefore, a coupling agent is necessary to solve this; and the second is the low applicability of this precursor due to its high price and to the significant amount of silver present in the solution, joined to the reduced certainty of silver stability because no new chemical bonds were observed and there was no evidence on the formation of the NPs. Finally, Vallejo-Montesinos et al. [31] proposed a filler made with TiO_2 and AgNPs, finding that the particles modified by silanization support the integration within the matrix. Nevertheless, a considerable amount of $AgNO_3$ was required as the precursor of AgNPs which could cause saturation of the support, whereas the antimicrobial activity was tested on starch–chitosan films, presenting disadvantages and limitation because this material exhibits high affinity for moisture and low water stability attributed to its highly hydrophilic character, which makes its application not very feasible.

For all this, the aim of this work was to discuss the mechanism of Ag deposition on TiO_2, evaluating if the use of a coupling agent, organosilane, would

obtain more AgNPs, and indeed, it would enhance the antimicrobial activity of the functionalized metal oxide; for this purpose, Gram-positive and Gram-negative bacteria were tested by the disk diffusion method. In addition, it was assessed the proposal to confer this property to PLA by filling it with these NPs, which was evaluated by the drop test method; and finally how the mechanical properties are influenced with these fillers.

Materials and methods

Materials

Titanium dioxide (TiO_2) particles with an average diameter of 350 nm and a crystalline structure of rutile were obtained from DuPont (R-104 Dupont, Mexico). The coupling agent 3-aminopropyltriethoxysilane (APTES, 97% purity) was supplied by Sigma-Aldrich (Mexico). Calcium hydroxide ($Ca(OH)_2$, 98%) and poly(lactic acid) (3.3 relative viscosity, 15 Melt flow index, and 1.24 specific gravity) were supplied by 3M Company Mexico; and silver nitrate ($AgNO_3$, 99.3%) was supplied by Fermont.

Functionalization of TiO_2 nanoparticles with APTES

TiO_2 was superficially modified with APTES in a 5:1 proportion. TiO_2 was mixed with ethanol and stirred for 30 min and then sonicated for 30 min at 60 Hz in an ultrasonic bath; this procedure was repeated until completing 2.5 h. Subsequently, APTES was added and stirred overnight. The solution was washed by centrifugation with water twice and with methanol five times, with the aim of removing the unreacted agent. Drying was carried out in an oven at 80 °C for 3 h. The dried powder was stored in vials for further testing and labeled as $sTiO_2$.

Preparation of Ag-deposited TiO_2 nanoparticles

TiO_2 was mixed with water and sonicated for 5 min at 60 Hz in an ultrasonic bath; then, heated to 80 °C; and while stirring, $AgNO_3$ was added (at different percentages 10%, 20%, and 30% w/w). The pH was adjusted to 12 with NaOH (0.5 M), and each mixture was stirred for 2 h. Each solution was washed with water by centrifugation five times, in order to remove the unreacted agent. Drying was carried out in an oven at 80 °C until the water evaporated. The dried powder was stored in vials for further testing, and the vials were labeled as TiO_2–Ag 10%, TiO_2–Ag 20%, and TiO_2–Ag 30%, respectively. The above procedure was repeated for the TiO_2 functionalized with APTES ($sTiO_2$), and the obtained products were labeled as $sTiO_2$–Ag 10%, $sTiO_2$–Ag 20%, and $sTiO_2$–Ag 30%, respectively.

Characterization of Ag-deposited TiO_2 nanoparticles

Scanning transmission electron microscopy (sTEM) analysis was performed to confirm the superficial modification and the Ag deposition. The eight samples TiO_2, $sTiO_2$, TiO_2–Ag (at 10%, 20%, and 30% w/w), and $sTiO_2$–Ag (at 10%, 20%, and 30%) were dispersed in an aqueous medium, making serial dilutions until achieving the optimum particle concentration. A drop was placed on a copper grid and observed in a JEOL equipment (model JEM 1230 microscope) with a resolution of 0.4 nm and an acceleration voltage of 100 kV.

X-ray photoelectron spectroscopy (XPS) was used to measure the chemical surface composition of the material and the chemical and electronic state of the elements that compose the surface. For the XPS analysis, an ultra-high vacuum (UHV) system from PerkinElmer PHI5100 was used with an SCA 10-360 analyzer detector. A dual X-ray source of Mg Kα ($h\nu = 1256$ eV) at 300 W and 20 mA beam intensity was used, with a polarized anode at 15.0 kV. The XPS spectrum was obtained at 54° from normal to the surface with a constant energy step (CAE) $E_0 = 71.55$ eV for the full scan spectrum and $E_0 = 22.36$ eV for high-resolution spectra. The pressure was maintained, during measurement, at 1×10^{-8} Torr. The energy position was calibrated with the Ag $3d_{5/2}$ orbital at the position of 368.20 eV with a resolution (FWHM) of 1.10 eV, Au $4f_{7/2}$ at 84.00 eV, and C 1*s* at 284.75 eV. Elemental composition analysis was performed using as a basis for the relative sensitivity factor reported by Scofield [30].

Antimicrobial activity Ag-deposited TiO_2 nanoparticles by disk diffusion method

The antimicrobial activity of the eight systems TiO_2, $sTiO_2$, TiO_2–Ag (at 10%, 20%, and 30%), and $sTiO_2$–Ag (at 10%, 20%, and 30%) was evaluated by disk diffusion method [32] against bacteria Gram-positive (*Staphylococcus aureus*) and Gram-negative (*Escherichia coli*). The eight samples were sterilized in a 1 ppm solution with ethanol at 70% v/v. The disks were placed in vials and soaked with each freshly prepared system. Then, the disks were left to impregnate. The microbial strains of bacteria, *E. coli,* and *S. aureus*, were inoculated into nutrient broth and kept overnight for incubation in a furnace. The turbidity of broth cultures was compared with 0.5 McFarland solutions, corresponding to $1–2 \times 10^8$ colony-forming units (CFU mL^{-1}).

The solid growth medium used for *E. coli* and *S. aureus* was eosin methylene blue (EMB) and mannitol agar, respectively. Petri dishes were inoculated using a sterile swab with the microorganisms, rotating the box 60° for each striatum application. The inoculated dishes were let settle and dried for 15 min with the lid closed. Finally, the disks previously impregnated in each of the TiO_2 systems were placed on each dish. Petri dishes were incubated in a furnace at 37 °C for 24 h. Finally, the zones of inhibition (halo) of each system were measured under an extraction hood. The assays were performed in triplicate, and mean values of zone diameter were taken.

Preparation of PLA films with Ag-deposited TiO_2 nanoparticles

PLA/TiO_2, PLA/sTiO_2, PLA/TiO_2–Ag (at 10%, 20%, and 30%), and PLA/sTiO_2–Ag (at 10%, 20%, and 30%) nanocomposites at 1% w/w were prepared. 500 mg of PLA was dissolved in 20 mL of chloroform; once a homogeneous solution was obtained, 5 mg of NPs was added, and then stirred and sonicated for 30 min at 60 Hz in an ultrasonic bath. The suspension obtained was placed on a glass container (silica), and the solvent was allowed to evaporate at room temperature overnight with the purpose of obtaining the film. This procedure was made for each system of nanoparticles.

Antibacterial analysis of PLA films by drop test method

PLA and its composites, PLA/TiO_2, PLA/TiO_2–Ag 10%, PLA/TiO_2–Ag 20%, PLA/TiO_2–Ag 30%, PLA/sTiO_2, PLA/sTiO_2–Ag 10%, PLA/sTiO_2–Ag 20%, and PLA/sTiO_2–Ag 30%, were tested against *E. coli* or *S. aureus* using the antibacterial drop test method with some modifications [22]. The same inoculated microbial strains of bacteria were used as for the disk method. A film of each respective composite was introduced in a different test tube, in triplicate, each one containing nutrient broth inoculated with the respective bacteria, Gram-positive and Gram-negative. Moreover, a film of pure PLA was used as a positive control, and a culture of each microorganism was grown without any treatment as a negative control. Then, the tubes were incubated for 24 h, and the solutions were read with a spectrophotometer. The optical absorptions $[A]$ were obtained, and the inhibition rate (%) was calculated as follows:

$$\text{Inhibition rate}\,(\%) = \frac{[A]_i - [A]_c}{[A]_i} \times 100 \tag{1}$$

where $[A]_i$ is the optical absorption of untreated bacteria and $[A]_c$ is the absorption of each composite.

Effect of Ag-deposited TiO_2 nanoparticles in PLA films under mechanical properties

The mechanical tests of PLA and composites PLA/TiO_2, PLA/TiO_2–Ag 10%, PLA/TiO_2–Ag 20%, PLA/TiO_2–Ag 30%, PLA/sTiO_2, PLA/sTiO_2–Ag 10%, PLA/sTiO_2–Ag 20%, and PLA/sTiO_2–Ag 30% were determined using an INSTRON universal machine model 3369 with a charge of 50 kN and a jaw separation speed of 25 m min^{-1}. Tensile stress and Young's modulus values were recorded with the aim of knowing the capacity at which materials will maintain the integrity and resistance during handling.

Evaluation of ion release by ICP-MS

One sample of each composite (PLA and PLA/TiO_2 and PLA/sTiO_2 at each concentration) was immersed in deionized water and sonicated for 30 min at 60 Hz in an ultrasonic bath, and then 2% of HNO_3 was added. The amounts of released titanium and silver ions were determined by analyzing the resulting solutions using an inductively coupled plasma mass spectroscopy (Model X, Series 2 ICP-MS by Thermo Electron Corporation); this spectrophotometer detects ions in each mass in a rapid sequence, allowing the individual isotopes of an element to be determined. The electrical signals resulting from the detection of the ions are processed within the digital information that is used to indicate the intensity of the ion and, subsequently, the concentration of the element.

Evaluation of cell viability

Cell viability was investigated by seeding peripheral blood mononuclear cells (PBMC) in 96-well plates (Costar, Corning, NY, USA) at a cell density of 3×10^4 cells per well in RPMI-1640 medium (supplemented with 10% fetal bovine serum, 2 mM l^{-1} glutamine, 50 U ml^{-1} penicillin, and 50 mg ml^{-1} streptomycin; Gibco-Invitrogen Corp., Carlsbad, CA, USA). The mononuclear cells were exposed to different concentrations (5% and 11% v/v) of the solutions resulting from each composite; these solutions were obtained the same as in the ICP-MS analysis and were cultured for 24 h at 37 °C in an atmosphere of 5% CO_2 and 95% relative humidity. After this time, the cells were treated with resazurin (Sigma-Aldrich, St. Louis, MO, USA) at 30 µg ml^{-1} diluted in RPMI medium in a final volume of 100 µl per well. Plates were incubated immediately for 2 h at 37 °C and 5% CO_2 atmosphere and protected from light. Fluorescent measurements with an excitation wavelength $\lambda=560$ nm and an emission wavelength $\lambda=590$ nm were performed with the objective of determining the degree of metabolism of resazurin in a Spectrofluorometer Synergy H1 (BioTek Instruments Inc. Winooski, VT, USA). Untreated PMBC was used as a negative control, and cells treated with acetone (10%) were set as a positive control (Sigma-Aldrich, St. Louis, MO, USA).

Cell viability of all dosing treatments was determined in triplicate using the following equation:

$$\text{Cell viability}\,(\%) = \frac{F_S}{F_C} \times 100\% \tag{2}$$

where F_s is the fluorescence value of each sample and F_C is the fluorescence of the control.

Results and discussion

sTEM analysis of Ag-deposited TiO_2 nanoparticles

sTEM was used to confirm both the Ag deposition and the chemical modification of TiO_2 with APTES. The image corresponding to the system TiO_2–Ag 30% is shown in Fig. 1; as can be seen, there are TiO_2 particles with a size of 100–180 nm, forming agglomerates due to their high density; also, it is possible to observe small particles of Si, incrusted on the TiO_2 particles of size between 15 and 35 nm, and finally small dots of Ag of 5–11 nm are observed in all the agglomerates. With the goal of quantifying the amount of Ag deposited, an elemental analysis with the help of energy-dispersive X-ray spectroscopy (EDS) was performed; the results are observed in Fig. 2, and the amount of each element is listed in Table 1, in which 1.2% of Ag was measured in the whole system of TiO_2–Ag 30%. On the other hand, Fig. 3 shows the image for sTiO_2–Ag 30%, which reveals an APTES organic coating on the TiO_2 surface of around 25 and 30 nm; actually, these particles present a better dispersion since no large agglomerates are observed, agreeing with previous investigations [25]; finally, more dots of Ag are observed than in the previous system but of equal size. The results of EDS analysis (Fig. 4) showed that more Ag was deposited in the sTiO_2–Ag 30% system, measuring up to 7.4%. According to both tests, sTEM and EDS, Ag was observed attached to the Si atoms; therefore, the silanized system, sTiO_2–Ag 30%, improved the deposition of Ag since more Si atoms (22.6% according to EDS) are presented in the surface of the oxide. It is important to measure that sTEM at high magnification is a more or less surface-related analytical tool. As a result, only a limited number of particles can be detected or visualized in such a small volume, and the limit of detection is therefore high. Energy-dispersive X-ray

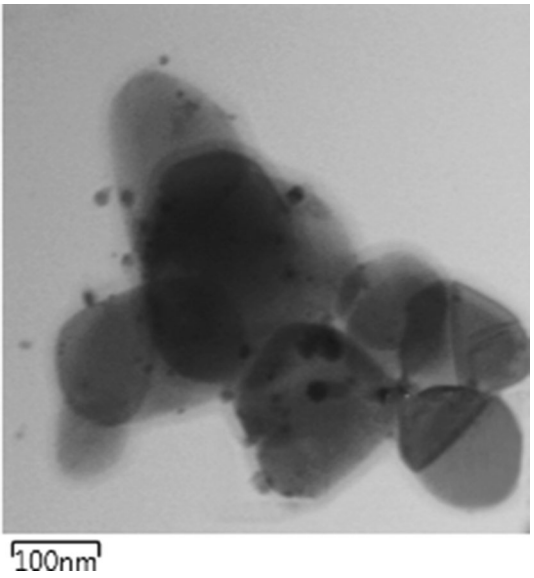

Fig. 1 sTEM images for TiO_2–Ag 30%

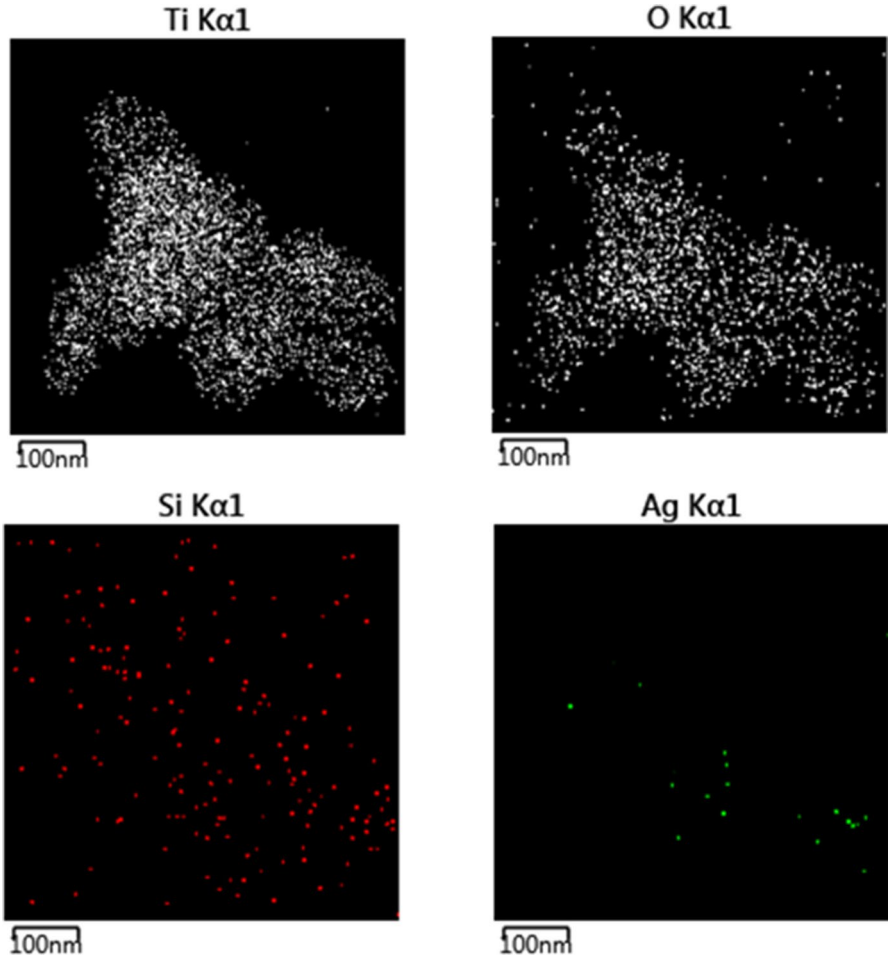

Fig. 2 EDS analysis for TiO_2–Ag 30%

Table 1 Weight % of elements in TiO_2–Ag 30% and TiO_2–Ag 30% systems obtained from EDS

Element	System	
	TiO_2–Ag 30% (%)	sTiO_2–Ag 30% (%)
Ti	62.2	48.8
O	34.4	21.3
Si	2.2	22.6
Ag	1.2	7.4

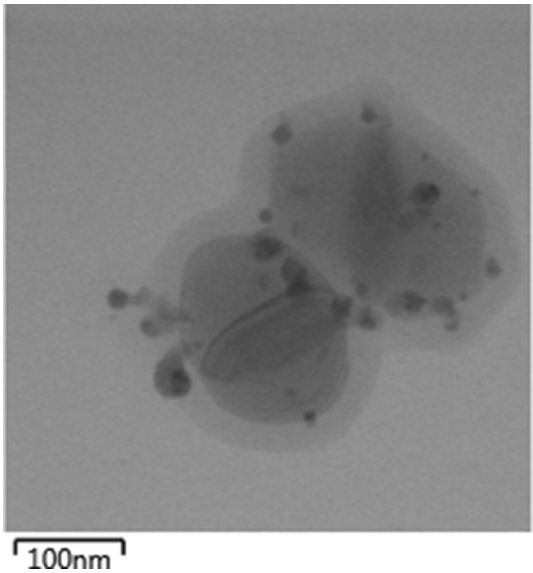

Fig. 3 sTEM images for $sTiO_2$–Ag 30%

spectroscopy (EDS or EDX) become even more important tool for the determination of elemental composition of the observed samples [33]. This means that through this technique (sTEM), it is possible to obtain an approximate concentration of the analyzed surface. Nevertheless, the main concern for this investigation is to fully know how the AgNPs were deposited and how TiO_2 was superficially modified with the coupling agent APTES and with the variation of the $AgNO_3$ amount. This was possible to observe by means of X-ray photoelectron spectroscopy (XPS), an analysis that allows to measure the chemical surface composition, the binding, and the chemical and electronic state of the elements that compose the surface.

Characterization of Ag-deposited TiO_2 nanoparticles by XPS

X-ray photoelectron spectrometry was carried out in order to further investigate the binding between Ti and Ag atoms on the surfaces of the TiO_2 and $sTiO_2$ systems: TiO_2–Ag 20%, TiO_2–Ag 30%, $sTiO_2$–Ag 20%, and $sTiO_2$–Ag 30%. Deconvolution analysis of XPS raw spectra was performed to estimate the presence of all species of each element. First, the XPS results for TiO_2 (Fig. 5a) and $sTiO_2$ (Fig. 5d) are compared, which show the Ti 2*p* core-level spectrum as two peaks at 464.5 and 458.8 e.V. for neat TiO_2 and at 464.3 and 458.7 e.V. for silanized TiO_2. These intense peaks can be assigned to the spin-orbital splitting of the Ti $2p_{1/2}$ and Ti $2p_{3/2}$, respectively; and it is important to point out that the distance between them is ~ 5.7 e.V.; all this proves clearly that this element consists of Ti^{4+} species on the sample surface [34–37]. This oxidation state for titanium is the most common in TiO_2; and according to the literature [38, 39], this is due to its route of synthesis (chlorination). In Fig. 5d, it is possible to observe that after the functionalization with APTES the titanium signals shift to a slightly lower B.E. (~ 0.2 eV), which is indicative of

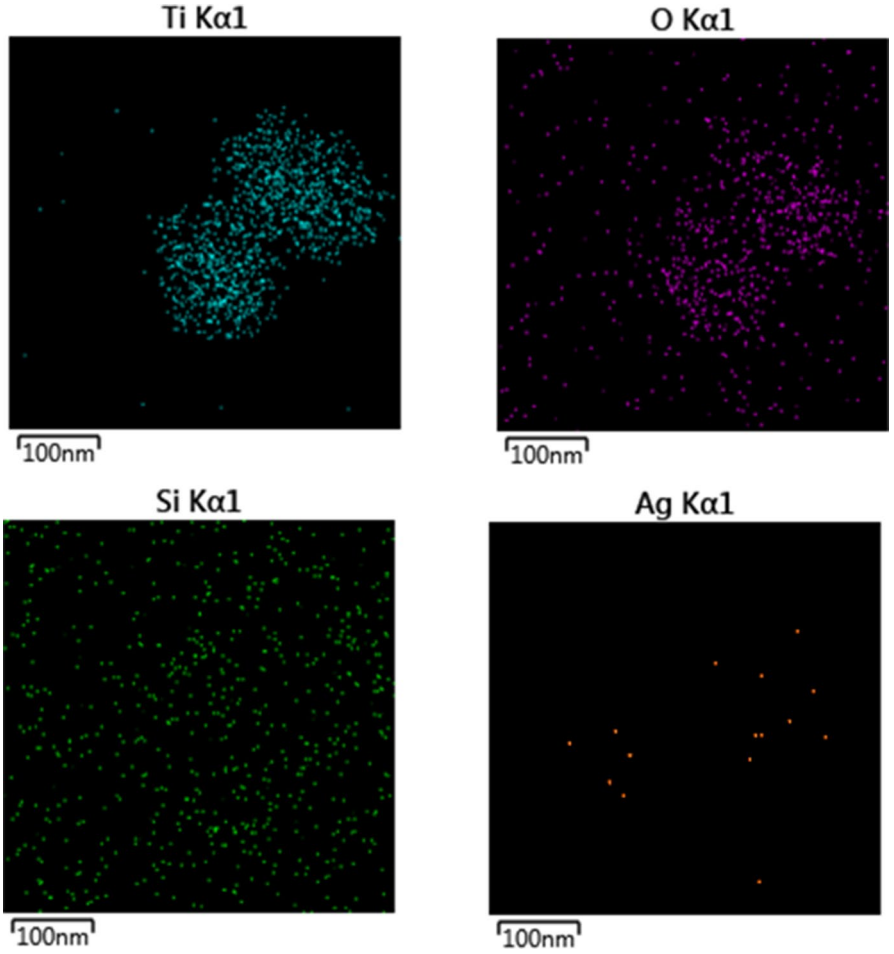

Fig. 4 EDS analysis for $sTiO_2$–Ag 30%

more electron-rich Ti atoms [40], and therefore, this surface improves its capacity to donate electrons allowing more deposition of AgNPs, which is shown in Fig. 8.

When Fig. 5a is compared to the results obtained for the Ag-deposited systems, the binding energy at Ti 2*p* increases as the amount of $AgNO_3$ (precursor) is added in the system, shifting in 0.3 e.V. for TiO_2–Ag 20% (Fig. 5b) and in 1.2 e.V. for TiO_2–Ag 30% (Fig. 5c); and for the silanized system (Fig. 5d) in 0.9 e.V. for $sTiO_2$–Ag 20% (Fig. 5e) and in 1.2 e.V. for $sTiO_2$–Ag 30% (Fig. 5f). According to the literature [41, 42], this phenomenon is because the Fermi level of Ag is lower than that of TiO_2, which results in a decrease in the outer electron cloud density of Ti ions and therefore in an increase in binding energy. On the other hand, it is possible to see that the Ti spectra for the Ag-deposited systems (Fig. 5b, c, e, f) present a new peak at ~ 461 e.V. and a flattening in the signals at ~ 464 and ~ 468 e.V.; this

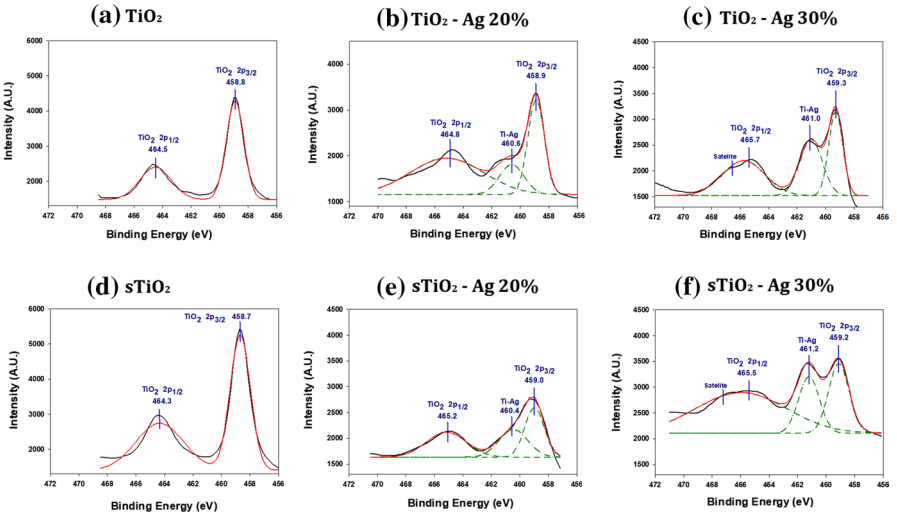

Fig. 5 XPS spectra for Ti element

could be interpreted as the partial reduction of the Ti on the surface after metal position, which is the production of a metal–metal bonding between Ag and Ti [43, 44].

Meanwhile in Fig. 6, the XPS spectrum of O1*s* for pure TiO_2 shows an asymmetric peak related to different chemical states. The characteristic peaks indicate that the value at ~ 530 e.V. is attributed to metal oxides (Ti–O–Ti) [42], and the peak at ~ 532 e.V. corresponds to the hydroxyl group (–OH) [45]. After silanization, it is observed a decrease in the B.E. (~ 0.2 eV) and in the intensity of the Ti–O–Ti

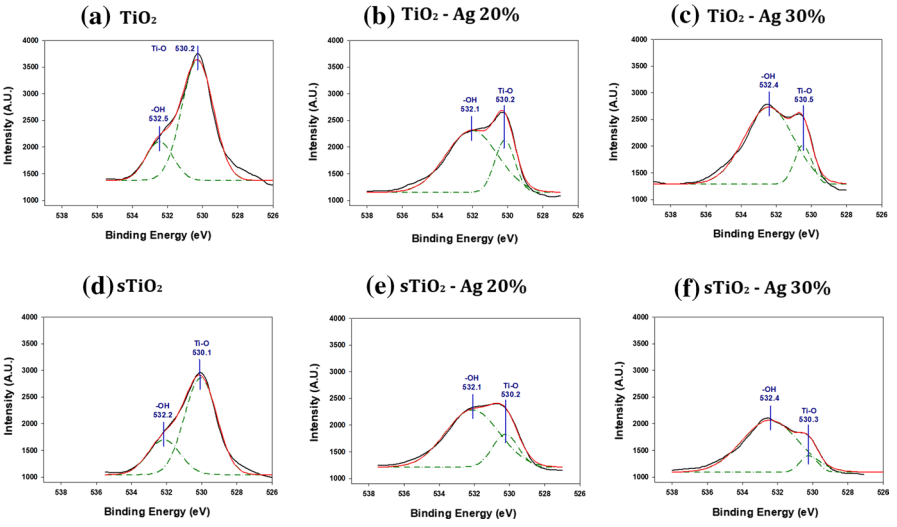

Fig. 6 XPS spectra for O element

Table 2 XPS results of TiO_2, $sTiO_2$ and Ag-deposited TiO_2 systems

Element	Specie	System					
		TiO_2 (%)	$sTiO_2$ (%)	TiO_2–Ag 20% (%)	TiO_2–Ag 30% (%)	$sTiO_2$–Ag 20% (%)	$sTiO_2$–Ag 30% (%)
C	Adventitious carbon	36.3	20.5	–	–	–	–
	C–O–C	39.7	43.7	71.2	46.1	39.0	50.0
	Oxidant carbon	24.0	35.7	17.4	23.7	36.9	19.0
	Carboxyl carbon	–	–	11.4	30.3	24.1	31.0
O	–OH	21.9	26.7	75.4	84.9	78.3	90.8
	O–Ti	78.1	73.3	24.6	15.1	21.7	9.2
Ti	TiO_2 $2p_{1/2}$	36.9	45.2	56.6	37.9	36.2	58.5
	TiO_2 $2p_{3/2}$	63.1	54.8	31.4	30.0	34.9	22.7
	Ti–Ag	–	–	15.0	32.2	28.9	18.8
Ag	Ag $3d_{3/2}$	–	–	18.9	15.3	15.5	17.3
	Ag $3d_{5/2}$	–	–	30.0	21.5	31.8	22.5
	Ag–Ti $3d_{5/2}$	–	–	26.1	35.4	21.8	33.2
	Ag–Ti $3d_{3/2}$	–	–	25.0	27.8	30.9	27.0

signal for the oxide functionalized with APTES, while according to the results in Table 2, the relative intensity of the hydroxyl group (–OH) increased by 4.8%; this indicates that the oxygen was changed from Ti–O–Ti into the chemical state of the hydroxyl state (–OH) [45]. This is likely due to surface band bending, which determines the formation of a negative space charge layer and implies that Ti^{4+} ions achieve a more reduced state [40]. Regarding the Ag-deposited systems (20% and 30%), the intensity of –OH peaks enlarged as the w/w concentration of $AgNO_3$ (precursor) increased, in 53.5% for TiO_2–Ag 20%, 63.0% for TiO_2–Ag 30%, and for the silanized systems in 56.5% for $sTiO_2$–Ag 20% and 68.9% for $sTiO_2$–Ag 30%, which possibly favors the oxidation processes on the TiO_2 surface with the production of reactive oxygen species (ROS) [46].

Regarding the C1s core-level spectra in Fig. 7, three peaks were shown at ~ 283, ~ 285, and ~ 286 e.V. in the TiO_2 and $sTiO_2$ systems, which are attributed to an adventitious carbon, C–O–C bond, and oxidant carbon such as alcohols, respectively, which are particularly frequent on reactive titanium surfaces [47]. The relative intensity of the C–O–C increased by four units after the silanization process; according to this, it is inferred that the carbon that exists near the oxygen in the (Ti–O) on the TiO_2 surface changed into the carbon that exists near the hydrogen in the Ti–OH bound [45].

As can be seen in Fig. 8, Ag signals were found only in the deposited systems exhibiting two characteristic peaks for the Ag 3*d* spectrum. The binding energy at ~ 374 e.V. corresponds to Ag $3d_{3/2}$, while the second peak at ~ 368 e.V. is for Ag $3d_{5/2}$, suggesting the presence of Ag^0 (368.2 eV) [42, 48]. The results of this study, together with sTEM and EDS analysis, indicate the presence of metal Ag-deposited systems. It is important to mention that there are no remains of precursor $AgNO_3$

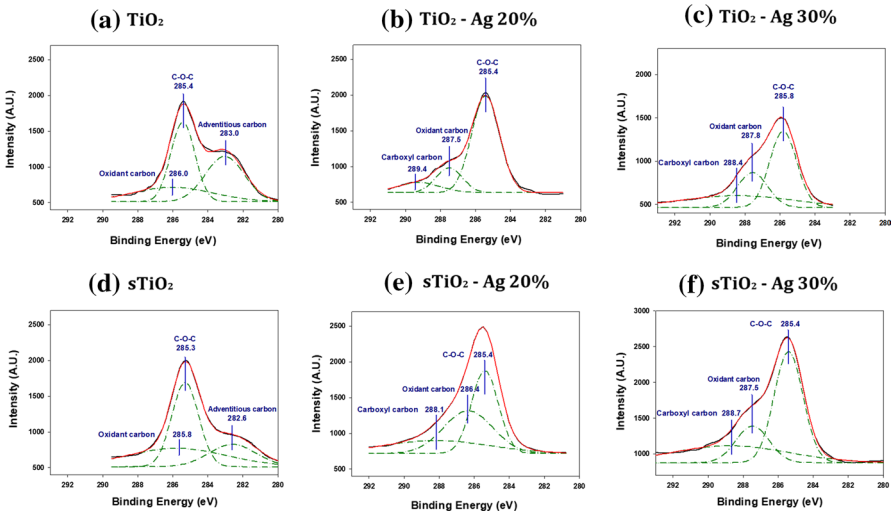

Fig. 7 XPS spectra for C element

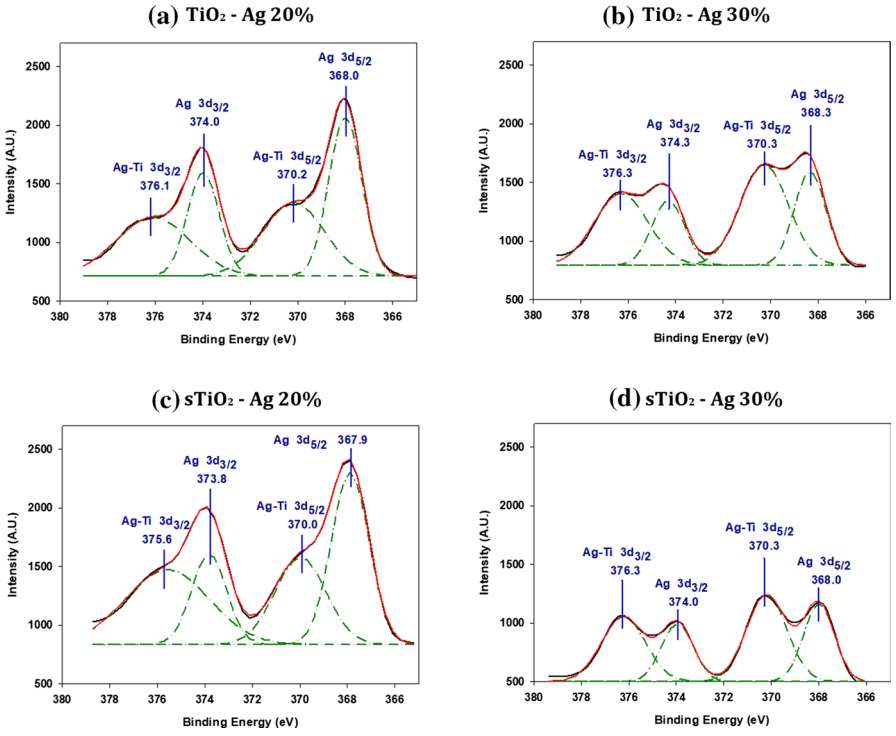

Fig. 8 XPS spectra for Ag element

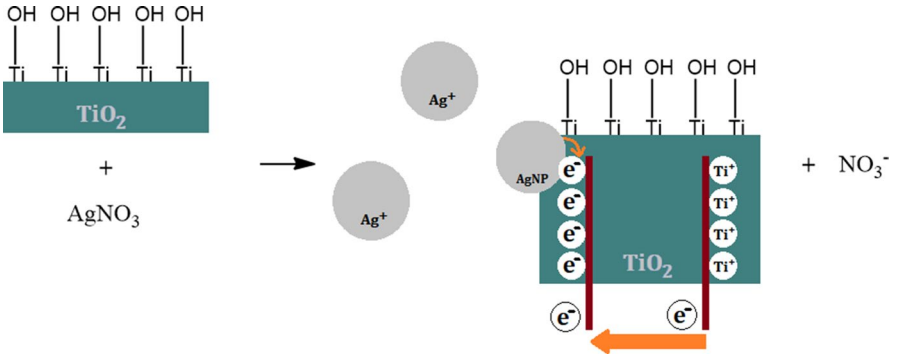

Fig. 9 Proposed reaction mechanism of Ag deposition on neat titanium dioxide (TiO_2)

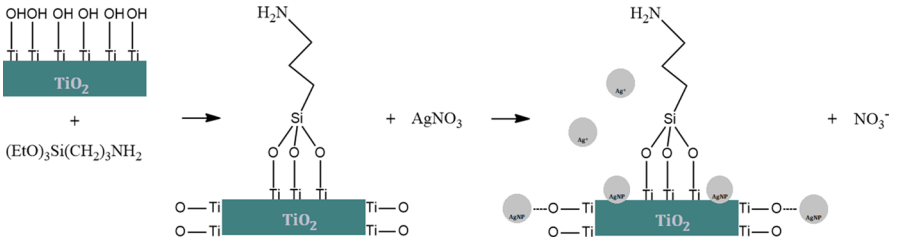

Fig. 10 Proposed reaction mechanism of Ag deposition on silanized titanium dioxide ($sTiO_2$)

since nitrogen was not detected at ~400 e.V. [49]. On the other hand, for the 20% and 30% systems, it was possible to observe two forming peaks at ~376 and ~370 e.V., respectively; these peaks are not an indicator of silver oxidation, but the Ti partial reduction due to the bond of Ag–Ti [44, 50]. This can be explained as the breaking of the original bonds with metal oxides, and the subsequent formation of new ones with silver (AgO), as confirmed by the appearance of peaks at ~376 and ~370 e.V., which is confirmed in Fig. 8b and d with the systems exhibiting an increase in these Ag–Ti peaks and higher ratios regarding Ag species (Ag–Ti/Ag): 51.1% for TiO_2–Ag 20%, 63.2% for TiO_2–Ag 30%, 52.7% for $sTiO_2$–Ag 20%, and 60.2% for TiO_2–Ag 30%).

Proposed reaction mechanism of Ag-deposited TiO_2

According to the results of the sTEM and XPS tests, it is possible to propose two reaction mechanisms for Ag deposition. The first one is for non-functionalized titanium dioxide, illustrated in Fig. 9, where the Ag nanoparticles have been deposited on the TiO_2 surface through a reduction in an $AgNO_3$ solution:

$$TiO_2 + AgNO_3 \rightarrow TiO_2 \cdot AgNP + NO_3^-$$

Silver ions in the vicinity of the TiO_2 surface capture electrons from titanium and deposit on the surface in the form of silver nanoparticles, creating Ti–Ag bonds.

When TiO_2 was silanized with APTES (Fig. 10), hydroxyl groups (–OH) were formed originating more active sites; therefore, the original bond Ti–O–Ti was broken, and silver oxide was formed (Ag–O). With this mechanism, more Ag could be deposited on the surface of TiO_2.

Thus, the presence of AgNPs on the TiO_2 surface favors oxidation processes on the TiO_2 surface with the production of reactive oxygen species (ROS), including the superoxide ion (O_2^-) and hydroxyl radical (OH) [46]. It is well known that the cell membrane of the bacteria has a negative charge due to the presence of lipids, carboxyl, phosphate, and amino groups; therefore, it attracts Ag^+ ions released from AgNPs due to electrostatic forces. This interaction of positive ions with phospholipid bilayer results in altering cell membrane permeability and reduction in the elastic modulus, extracellular products leak in, and intracellular contents leak out, ROS are generated, and finally, the microorganism dies (Fig. 11).

Antimicrobial activity of Ag-deposited TiO_2 nanoparticles by disk diffusion method

The antimicrobial activity of the disks impregnated with the systems was assessed on two bacteria, *E. coli* and *S. aureus,* under the disk diffusion method. The paper disk diffusion method is excellent for determining the susceptibility of bacteria to antibiotics and bactericidal agents [51], this is based on the presence or the absence of a zone of inhibition. For determining antimicrobial susceptibility, an acceptable disk diffusion method should be based not only on the presence or absence of a zone of inhibition but also on the size of the inhibition zone. Reliable results can only be obtained with disk diffusion tests that use the principle of standardized methodology

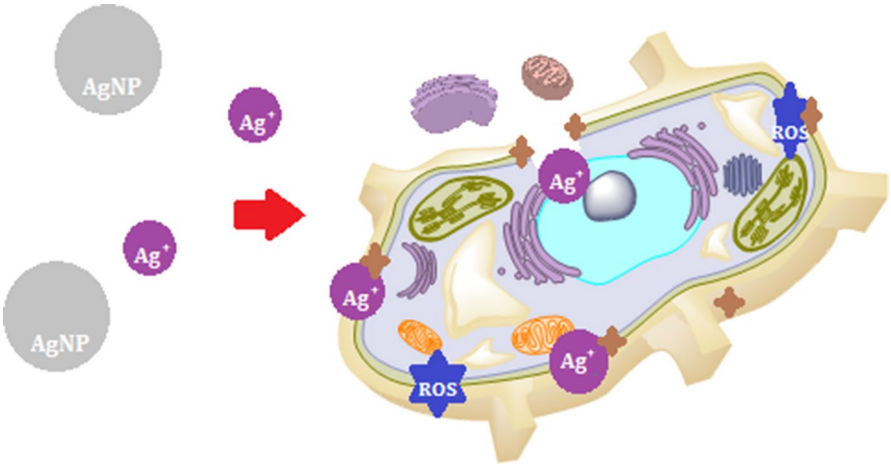

Fig. 11 Schematic mechanisms for antimicrobial effect of the AgNPs

and zone diameter measurements with strains known to be susceptible or resistant to various antimicrobial agents [52].

The measurements of inhibition zone in diameter (mm) around the impregnated disks are shown in Table 3. The results revealed that the Ag-deposited systems had an antimicrobial effect when compared to titanium dioxide, TiO_2, $sTiO_2$. It is clearly observed an increment in the inhibition zone for the silanized systems, and the best results were obtained for the $sTiO_2$–Ag 30%, system with inhibitions diameter of 10.6 mm for *S. aureus* and 18.4 mm for *E. coli*. This is attributable to this system that had more Ag content, according to the sTEM and EDS analysis, in comparison with the other systems. Yallappa et al. [53] performed a disk diffusion method to measure the antibacterial activity of Au, Ag, and Au–Ag alloy nanoparticles, using erythromycin (10 µg/disk) as organic antimicrobial standard. The antimicrobial zone of inhibition of the standard was 8 and 13 mm to *S. aureus* and *E. coli*, respectively. This means that the results of $sTiO_2$–Ag 30% (silanized system) on *S. aureus* (10.6 mm) and *E. coli* (18.4 mm) are above the inhibition range.

This bactericidal effect was caused by Ag^+ ions, which interact with bacterial cells and adhere to the bacterial walls [17] affecting the peptidoglycan cell wall and plasma membrane, bacterial DNA, and bacterial protein, particularly enzymes [5, 13]; on the other side, the effect of concentration in the system is clearly noted; a higher percentage (20–30%) of Ag increased the inhibition zone for both bacteria. It is noteworthy that silanized systems enhanced antimicrobial effect for Ag-deposited TiO_2; this can be attributed to silane agent that provides a better dispersion of the Ag and TiO_2, not only generating a high surface area, which caused a high antimicrobial efficiency of these nanoparticles [53] but also electrostatic forces between bacteria and Ag^+ ions improving their adhesion [17].

Analysis of films by antibacterial drop test method

The films obtained following "Preparation of PLA films with Ag-deposited TiO_2 nanoparticles" section for the different systems are shown in Fig. 12. According to the drop test method described in "Antibacterial analysis of PLA films by drop test method" section, it was possible to observe clearly the antibacterial activity for the PLA composites filled with Ag-deposited TiO_2. As observed in Fig. 13, the results indicated that the antimicrobial activity of PLA/TiO_2–Ag is attributed to the AgNPs deposited on TiO_2 surface, since a better inhibition rate is observed

Table 3 Antibacterial activity of $sTiO_2$, TiO_2 and Ag-deposited TiO_2 by Disk diffusion method

Microorganisms	Mean zone of inhibition (mm)							
	TiO_2	$sTiO_2$	10% w/w		20% w/w		30% w/w	
			TiO_2–Ag	$sTiO_2$–Ag	TiO_2–Ag	$sTiO_2$–Ag	TiO_2–Ag	$sTiO_2$–Ag
S. aureus	ND	ND	ND	ND	ND	ND	9.1	10.6
E. coli	ND	ND	ND	ND	ND	12.4	11.2	18.4

ND not detected

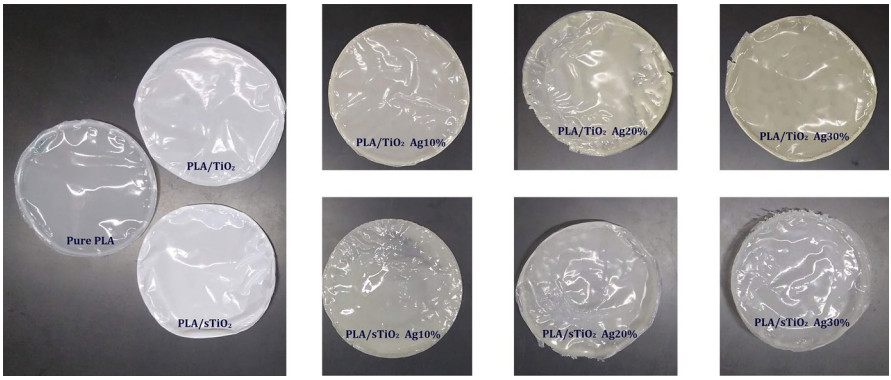

Fig. 12 Films of PLA and its composites

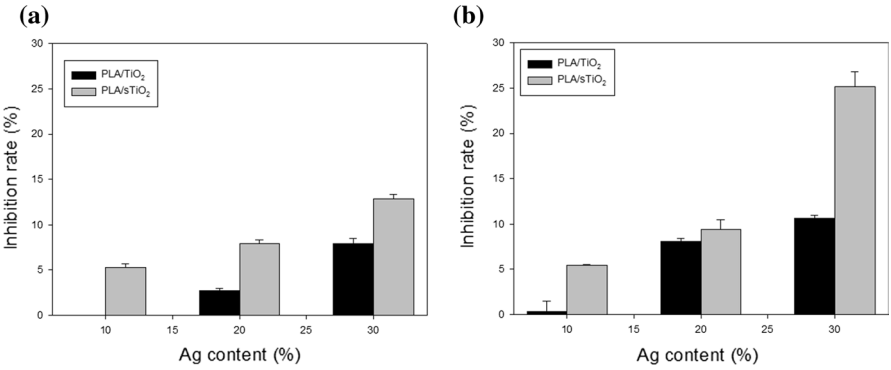

Fig. 13 Inhibition rates for **a** *E. coli* and **b** *S. aureus* as a function of Ag content for PLA composites

when the Ag content increased. The results of the inhibition rate are shown in Fig. 13a for *E. coli* and in Fig. 13b for *S. aureus*.

As observed, the inhibitory effect of PLA/TiO_2–Ag and PLA/sTiO_2–Ag films for *S. aureus* was stronger than that for *E. coli*. This can be attributed to the fact that the wall of Gram-positive cells contains a thick layer and, conversely, Gram-negative cell walls are more complex since this cell contains a thin membrane and an outer membrane, which cover the wall of the surface and confer resistance to hydrophobic compounds. Therefore, the structure of the cell wall plays an important role in the susceptibility of bacteria in the presence of AgNPs [22, 54]. Finally, it is possible to conclude that the best inhibitory rate was obtained again for the systems with silanized TiO_2, especially for the PLA/sTiO_2–Ag at 30%, thanks to the greater presence of AgNPs in the filler. In this case, the antibacterial effect was caused by contact with silver, since previous trials of disk diffusion method using the polymer composites as disks on agar did not show inhibition zone, while in the drop test method, a clear inhibition was found.

The antimicrobial effect of AgNPs is known to be greatly influenced by the type and size of the AgNPs and the uncontrolled release of AgNPs or silver ions from the carrier matrices. Therefore, in the PLA/TiO_2–Ag composites, non-functionalized and silanized, the polymer matrices can help to control the release of silver ions by altering the interactions between AgNPs and polymeric materials [55]. These findings are consistent with other studies. In LDPE–silver nanocomposites, clear inhibition zone of 10.71 and 1.52 mm was observed by agar diffusion test to *S. aureus* and *E. coli*, respectively [56]. In cellulose–AgNPs nanocomposites, the inhibition zone of nanocomposites active films was 3.11 and 2.75 mm to *S. aureus* and *E. coli*, respectively; they indicated that Gram-positive strains are more sensitive to silver compounds than Gram-negative bacteria, which attributed to binding of silver ions to peptidoglycan layer [57]. More oxygen vacancies on the TiO_2 surface increase the nucleation of metallic AgNPs, besides TiO_2 contributing to the improvement in physical and mechanical properties on fillers. Previous studies reported the enhancement of antibacterial activity by synergistic effect between Ag and metal oxides, which could be mainly due to the increase in the generation of the reactive oxidative species (especially superoxide) and the increased damage to plasmid DNA induced by AgNPs [58].

Effect of Ag-deposited TiO_2 nanoparticles under mechanical properties

In order to investigate the effect of nanoparticles on the mechanical properties of PLA film, especially the effect of silanization on the TiO_2 particles in the tensile stress and Young's modulus tests, all composites were evaluated and the results are represented in Fig. 14. In this, it is possible to observe that the presence of NPs within the polymeric matrix increased the rigidity of the resulting composites, even just with the inclusion of TiO_2 without AgNPs; this improvement is due to the strong interfacial interaction between TiO_2 and polymeric matrix [22, 30].

In Fig. 14a, the values indicate that the presence of Ag has influence in the tensile stress test (Fig. 14a) since higher values were obtained when the concentration increased. However, for the highest percent of Ag (30%), there was a decrease in the value, probably to the excess of AgNPs that tend of agglomerate in the filler; also,

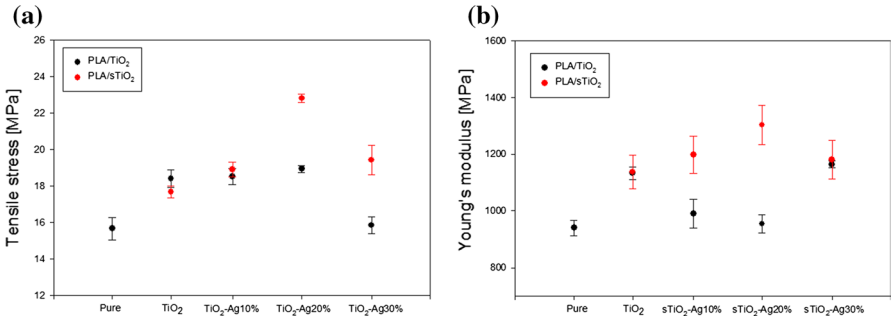

Fig. 14 Variation of **a** tensile stress and **b** Young's modulus as function of Ag content for PLA composites

this can be explained by the aggregation of TiO_2 in the matrix due to the interaction between the Ti–OH and Ti–Ag groups on the particle surfaces [9], especially for the non-silanized particles. It is essential to point out the higher values found for the systems silanized with APTES because this coupling agent improves the integration of the particles within the matrix thanks to the strong interfacial adhesion and better dispersion between the $sTiO_2$ nanoparticles [19, 30]. The best result was found for the composite PLA/$sTiO_2$–Ag 20% with an improvement of 45.7% in relation to pure PLA.

Similar behavior was observed for Young's modulus (Fig. 14b), in which the elasticity decreased as Ag content increased, exclusive for the composites with silanized particles, with the exception of PLA/$sTiO_2$–Ag 30%, while the non-silanized systems had less stiffness [59, 60] and practically exhibit the same values than pure PLA, except for the PLA/TiO_2–Ag 30%. The high values found in composites with silanized particles are an indicator that these particles make films harder [61], which makes the composite ideal for applications where a resistant material is required. The best improvement was in 38.73% for PLA/$sTiO_2$–Ag 20% composite. For all this, it is possible to state that it is widely demonstrated that the proper interactions between PLA chain molecules and AgNPs are due to the presence of van der Waals interactions between the hydroxyl groups of PLA and the partial positive charge on the surface of AgNPs [29] and that the silanized systems had better mechanical properties thanks to their terminal NH_2 groups, which form intermolecular hydrogen bonds with the OH– groups of the PLA [31].

Evaluation of ion release by ICP-MS

Table 4 shows the concentration of Ti and Ag ions released from each composite sample measured by ICP-MS. The presence of these ions is observed only in four composites and in very low concentrations. In PLA/TiO_2–Ag at 10 and 20%, the Ag release maybe is due to the incomplete efficiency reaction on metal nanostructures, such as long reaction time, for example, in previous investigation; there was observed oxidations of p-amino thiophenol (PATP) to p,p′dimercaptoazobenzene

Table 4 Concentration of ion release for composites by ICP-MS analysis

Composite	Ion concentration (ppb)	
	Ti	Ag
PLA	0	0
PLA/TiO_2	0	0
PLA/TiO_2–Ag 10%	0	3.4
PLA/TiO_2–Ag 20%	0	0.5
PLA/TiO_2–Ag 30%	0	0
PLA/$sTiO_2$	0	0
PLA/$sTiO_2$–Ag 10%	1.2	0
PLA/$sTiO_2$–Ag 20%	0	0
PLA/$sTiO_2$–Ag 30%	5.2	11.3

(DMAB) in Ag nanoparticles (AgNPs) and an incomplete reduction of 4-nitrobenzenethiol (4NBT) to DMAB on Ag nanoparticle film hybrid system or Ag nanowire-Au nanoparticle nanostructures [62]. While only Ti was slightly detected in the composites with $sTiO_2$–Ag but in scarce concentrations, the highest value of Ag ion was detected in the PLA/$sTiO_2$–Ag 30%; the composite with the highest amount of silver, but in a scarce value of ~ 11 ppb, may be due to excess silver not properly anchored to the TiO_2 surface. Although the silanized particle improves the AgNPs deposition, this reaction is limited by a certain number of sites in which the nanoparticle can interact with the OH residues of APTES, so the rest of the silver is distributed in the polymer matrix and migrate because it is not anchored to the support material. These results suggest that an intermediate concentration between 20 and 30% of AgNPs could give a better deposited–composite relation. All this achieves not only the non-toxicity of the composites but also a prolonged surface antibacterial effect [63].

Evaluation of cell viability

The cytotoxic effect of each resulting solution was evaluated on PBMBC at two different concentrations (5% and 11%) through Resazurin assay. Figure 15 shows the results for each composite, and according to this, it is possible to state that the resulting solutions do not have a negative effect on the PBMC viability for any treatment during 24 h of exposure, compared to the control sample. It is well known that the intrinsic properties of Ag-deposited TiO_2 nanoparticles, such as size, shape, and chemical composition, could correlate with the development of cytotoxic effects [64]. In this context, it has been observed that the nanoparticles that may enter the bloodstream and have direct contact with proteins and cells generate a reaction that decreases cell viability through oxidative stress and damages DNA, apoptosis, and others [65]; nevertheless, these resulting solutions did not exert a toxic effect since cell viability was above 80%, representing non-toxic conditions for cells, in accordance with ISO 10993-5:2009.

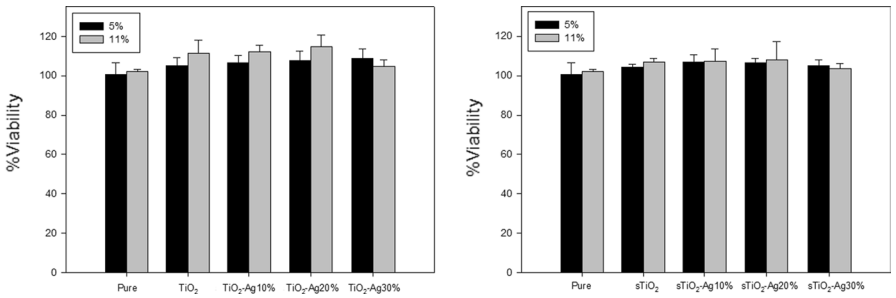

Fig. 15 Cell viability of PLA and its composites with **a** neat TiO_2 and **b** silanized TiO_2

Conclusions

In this work, pure and silanized titanium dioxide was deposited with AgNPsr by reduction of $AgNO_3$, testing three different concentrations (10%, 20%, and 30% w/w) of this precursor. The results of the sTEM analysis confirm the chemical modification of TiO_2 with APTES, since an organic coating on the TiO_2 surface of around 25 and 30 nm is observed in the $sTiO_2$ systems, which was not previously observed in pure TiO_2. The Ag deposition on the oxide particles was confirmed by the sTEM, XPS, and EDS analysis. With these results, it was possible to conclude that a higher amount of silver (7.4%) was present when the amount of $AgNO_3$ precursor was incremented and when the oxide was previously silanized, thanks to the silanization process that created more active sites on the TiO_2 surface, favoring the bound of silver.

Respect to the antimicrobial effect, favorable results were found in Ag-deposited TiO_2 nanoparticles since they showed antimicrobial activity against microorganisms such as *Staphylococcus aureus* and *Escherichia coli* at 20% and 30% w/w of $AgNO_3$ (precursor). It is clearly shown that there were better inhibition results when deposition was performed on titanium dioxide previously silanized, 14.2% for *S. aureus,* and 39.1% for *E. coli* in % inhibition rate. According to the results, it was possible to confer the antimicrobial property to PLA composites by incorporating Ag-deposited TiO_2 as filler, and the inhibition behavior was replicated according to what was observed for the silanized particles, showing enhancement in 57.6% for *S. aureus* and 38.8% for *E. coli*. Regarding mechanical properties, better properties were obtained when silanized particles were used as fillers, since higher results were obtained in the functionalized composites, in comparison with pure PLA. The best result was found for the PLA/$sTiO_2$–Ag 20% composite with an improvement of 45.7% for tensile stress and of 38.73% for Young's modulus. Therefore, these films are harder, making them ideal for applications where a tough material is required.

Finally, it was found that PLA composites with these nanoparticles are non-toxic because there is practically no migration of ions from the polymeric matrix, which helps to enhance the prolonged surface antibacterial effect. Therefore, in accordance with the favorable results of the research, a broad perspective is opened on the use of Ag-deposited TiO_2, previously silanized, to create antimicrobial and non-toxic PLA composites that can be used at the industrial and commercial levels in the medical, food, and agricultural field, in areas as water purification, the stability of liposomes, systems with photoactivation, biomolecules, drug encapsulation, environment, among others.

Acknowledgements The authors express their gratitude to Carlos Benavides Muñiz for experimental assistance in the microbial experiments. M.G. Peña-Juárez and J.A. Gonzalez-Calderón wish to thank Consejo Nacional de Ciencia y Tecnología (Conacyt México) for Ph.D. scholarship (No: 744689) and for the support with the program "Cátedras-Conacyt," respectively. R. Lopez-Esparza wishes to thank Universidad de Sonora by financial support through project USO315005347 and to Mora R. of the DIFUS by the assistance in XPS experiments.

Compliance with ethical standards

Conflict of interest The authors declare no conflicts of interest.

References

1. Södergård A, Stolt M (2002) Properties of lactic acid based polymers and their correlation with composition. Prog Polym Sci 27:1123–1163
2. Sánchez MS, Gómez Ribelles JL, Hernández Sánchez F, Mano JF (2005) On the kinetics of melting and crystallization of poly(l-lactic acid) by TMDSC. Thermochim Acta 430:201–210. https://doi.org/10.1016/j.tca.2005.01.066
3. Carrasco F, Pagès P, Gámez-Pérez J et al (2010) Processing of poly(lactic acid): characterization of chemical structure, thermal stability and mechanical properties. Polym Degrad Stab 95:116–125. https://doi.org/10.1016/J.POLYMDEGRADSTAB.2009.11.045
4. Kodal M, Wis AA, Ozkoc G (2018) The mechanical, thermal and morphological properties of γ-irradiated PLA/TAIC and PLA/OvPOSS. Radiat Phys Chem 153:214–225. https://doi.org/10.1016/j.radphyschem.2018.10.018
5. Siddiqi KS, ur Rahman A, Tajuddin A, Husen A (2018) Properties of zinc oxide nanoparticles and their activity against microbes. Nanoscale Res Lett 13:141. https://doi.org/10.1186/s11671-018-2532-3
6. Husen A (2017) Gold nanoparticles from plant system: synthesis, characterization and their application. Springer, Cham, pp 455–479
7. Robles-Martínez M, González JFC, Pérez-Vázquez FJ et al (2019) Antimycotic activity potentiation of *Allium sativum* extract and silver nanoparticles against *Trichophyton rubrum*. Chem Biodivers. https://doi.org/10.1002/cbdv.201800525
8. Kalayci OA, Cömert FB, Hazer B et al (2010) Synthesis, characterization, and antibacterial activity of metal nanoparticles embedded into amphiphilic comb-type graft copolymers. Polym Bull 65:215–226. https://doi.org/10.1007/s00289-009-0196-y
9. Li W, Zhang C, Chi H et al (2017) Development of antimicrobial packaging film made from poly(lactic acid) incorporating titanium dioxide and silver nanoparticles. Molecules 22:1170–1184. https://doi.org/10.3390/molecules22071170
10. Natarajan S, Bhuvaneshwari M, Lakshmi DS et al (2016) Antibacterial and antifouling activities of chitosan/TiO_2/Ag NPs nanocomposite films against packaged drinking water bacterial isolates. Environ Sci Pollut Res 23:19529–19540. https://doi.org/10.1007/s11356-016-7102-6
11. Li Y, Ma M, Chen W et al (2011) Preparation of Ag-doped TiO_2 nanoparticles by a miniemulsion method and their photoactivity in visible light illuminations. Mater Chem Phys 129:501–505. https://doi.org/10.1016/j.matchemphys.2011.04.055
12. Mukhopadhyay A, Basak S, Das JK et al (2010) Ag–TiO_2 nanoparticle codoped SiO_2 films on ZrO_2 barrier-coated glass substrates with antibacterial activity in ambient condition. ACS Appl Mater Interfaces 2:2540–2546. https://doi.org/10.1021/am100363d
13. Dhanalekshmi KI, Meena KS (2014) Comparison of antibacterial activities of Ag@TiO_2 and Ag@SiO_2 core–shell nanoparticles. Spectrochim Acta Part A Mol Biomol Spectrosc 128:887–890. https://doi.org/10.1016/j.saa.2014.02.063
14. Vallejo W, Díaz-Uribe C, Navarro K et al (2016) Estudio de la actividad antimicrobiana de películas delgadas de dióxido de titanio modificado con plata. Rev la Acad Colomb Ciencias Exactas, Físicas y Nat 40:69. https://doi.org/10.18257/raccefyn.289
15. Sabzi M, Mirabedini SM, Zohuriaan-Mehr J, Atai M (2009) Surface modification of TiO_2 nanoparticles with silane coupling agent and investigation of its effect on the properties of polyurethane composite coating. Prog Org Coat 65:222–228. https://doi.org/10.1016/j.porgcoat.2008.11.006
16. Angkaew S, Limsuwan P (2012) Preparation of silver–titanium dioxide core–shell (Ag@TiO_2) nanoparticles: effect of Ti–Ag mole ratio. Procedia Eng 32:649–655. https://doi.org/10.1016/j.proeng.2012.01.1322
17. Harikishore M, Sandhyarani M, Venkateswarlu K et al (2014) Effect of Ag doping on antibacterial and photocatalytic activity of nanocrystalline TiO_2. Procedia Mater Sci 6:557–566. https://doi.org/10.1016/j.mspro.2014.07.071

18. Alimunnisa J, Ravichandran K, Meena KS (2017) Synthesis and characterization of Ag@SiO2 core–shell nanoparticles for antibacterial and environmental applications. J Mol Liq 231:281–287. https://doi.org/10.1016/j.molliq.2017.01.103
19. Mendoza G, Peña-Juárez MG, Perez E, Gonzalez-Calderon JA (2020) Used of chemically modified titanium dioxide particles to mediate the non-isothermal cold crystallization of poly(latic acid). J Mex Chem Soc 64:44–63. https://doi.org/10.29356/jmcs.v64i2.1126
20. Delgado Alvarado E, Peña Juárez MG, Perez Perez C et al (2019) Improvement in the dispersion of TiO_2 particles inside chitosan-methyl cellulose films by the use of silane coupling agent. J Mex Chem Soc. https://doi.org/10.29356/jmcs.v63i2.741
21. Altan M, Yildirim H (2012) Mechanical and antibacterial properties of injection molded polypropylene/TiO_2 nano-composites: effects of surface modification. J Mater Sci Technol 28:686–692. https://doi.org/10.1016/S1005-0302(12)60116-9
22. Xing Y, Li X, Zhang L et al (2012) Effect of TiO_2 nanoparticles on the antibacterial and physical properties of polyethylene-based film. Prog Org Coat 73:219–224. https://doi.org/10.1016/j.porgcoat.2011.11.005
23. Luo YB, Da Li W, Wang XL et al (2009) Preparation and properties of nanocomposites based on poly(lactic acid) and functionalized TiO_2. Acta Mater 57:3182–3191. https://doi.org/10.1016/j.actamat.2009.03.022
24. Gonzalez-Rodriguez V, Escobar-Barrios V, Peña-Juárez MG, Pérez E (2020) Effect of aliphatic chain in dicarboxylic acids on non-isothermal crystallization and mechanical behavior of titanium dioxide/iPP composites. Thermochim Acta 686:178543. https://doi.org/10.1016/j.tca.2020.178543
25. López-Zamora L, Martínez-Martínez HN, González-Calderón JA (2018) Improvement of the colloidal stability of titanium dioxide particles in water through silicon based coupling agent. Mater Chem Phys 217:285–290. https://doi.org/10.1016/j.matchemphys.2018.06.063
26. Aragundy E, Salas V, Torres F (2011) Modificación de la Superficie del Titanio para Mejorar su Biocompatibilidad mediante la Aplicación de Técnicas de Recubrimiento con Aminas
27. Salleh E, Muhammad II, Pahlawi QA (2014) Spectrum activity and lauric acid release behaviour of antimicrobial starch-based film. Procedia Chem 9:11–22. https://doi.org/10.1016/j.proche.2014.05.003
28. Shameli K, Ahmad MB, Zin WM, Yunus W, Ibrahim NA, Maryam Jokar MD (2014) Synthesis and characterization of silver/polylactide nanocomposites. Mater Sci Forum 802:135–139. https://doi.org/10.4028/www.scientific.net/MSF.802.135
29. Da Silva EC, Da Silva MGA, Meneghetti SMP et al (2008) Synthesis of colloids based on gold nanoparticles dispersed in castor oil. J Nanopart Res 10:201–208. https://doi.org/10.1007/s11051-008-9483-z
30. De Silva RT, Pasbakhsh P, Lee SM, Kit AY (2015) ZnO deposited/encapsulated halloysite-poly (lactic acid) (PLA) nanocomposites for high performance packaging films with improved mechanical and antimicrobial properties. Appl Clay Sci 111:10–20. https://doi.org/10.1016/j.clay.2015.03.024
31. Vallejo-Montesinos J, Gámez-Cordero J, Zarraga R et al (2020) Influence of the surface modification of titanium dioxide nanoparticles TiO_2 under efficiency of silver nanodots deposition and its effect under the properties of starch–chitosan (SC) films. Polym Bull 77:107–133. https://doi.org/10.1007/s00289-019-02740-z
32. Maye Bernal R, Miguel Guzman U (1984) Antibiograma e discos normallzaclon de la tecnica de Kirby-Bauer. Biomedica. https://doi.org/10.7705/biomedica.v4i3-4.1891
33. Dudkiewicz A, Boxall ABA, Chaudhry Q et al (2015) Uncertainties of size measurements in electron microscopy characterization of nanomaterials in foods. Food Chem 176:472–479. https://doi.org/10.1016/j.foodchem.2014.12.071
34. Jensen H, Soloviev A, Li Z, Søgaard EG (2005) XPS and FTIR investigation of the surface properties of different prepared titania nano-powders. Appl Surf Sci 246:239–249. https://doi.org/10.1016/j.apsusc.2004.11.015
35. Akel S, Dillert R, Balayeva NO et al (2018) Ag/Ag_2O as a co-catalyst in TiO_2 photocatalysis: effect of the co-catalyst/photocatalyst mass ratio. Catalysts 8:1–19. https://doi.org/10.3390/catal8120647
36. Zhang Y, Fu F, Li Y et al (2018) One-step synthesis of Ag@TiO_2 nanoparticles for enhanced photocatalytic performance. Nanomaterials 8:1032. https://doi.org/10.3390/nano8121032
37. Mogal SI, Gandhi VG, Mishra M et al (2014) Single-step synthesis of silver-doped titanium dioxide: influence of silver on structural, textural, and photocatalytic properties. Ind Eng Chem Res 53:5749–5758. https://doi.org/10.1021/ie404230q

38. Koch D, Manzhos S (2017) On the charge state of titanium in titanium dioxide. J Phys Chem Lett 8:1593–1598. https://doi.org/10.1021/acs.jpclett.7b00313
39. Moodley S (2011) A study of the chlorination behaviour of various titania feedstocks, p 154
40. Meroni D, Lo Presti L, Di Liberto G et al (2017) A close look at the structure of the TiO_2-APTES interface in hybrid nanomaterials and its degradation pathway: an experimental and theoretical study. J Phys Chem C 121:430–440. https://doi.org/10.1021/acs.jpcc.6b10720
41. Ding Q, Zhang Z, Wang C et al (2012) Crystallization behavior and melting characteristics of wollastonite filled β-isotactic polypropylene composites. Thermochim Acta 536:47–54. https://doi.org/10.1016/J.TCA.2012.02.023
42. Xin B, Jing L, Ren Z et al (2005) Effects of simultaneously doped and deposited Ag on the photocatalytic activity and surface states of TiO_2. J Phys Chem B 109:2805–2809. https://doi.org/10.1021/jp0469618
43. Bahl MK, Tsai SC, Chung YW (1980) Auger and photoemission investigations of the platinum-$SrTiO_3$(100) interface: relaxation and chemical-shift effects. Phys Rev B 21:1344–1348. https://doi.org/10.1103/PhysRevB.21.1344
44. Masetti E, Bulir J, Gagliardi S et al (2004) Ellipsometric and XPS analysis of the interface between silver and SiO_2, TiO_2 and SiN_x thin films. Thin Solid Films 455–456:468–472. https://doi.org/10.1016/j.tsf.2003.11.244
45. Maruo YY, Yamada T, Tsuda M (2012) Reactivity of CO_2 and H_2O on TiO_2 catalysts studied by gas phase FT-IR method and deactivation mechanism. J Phys Conf Ser. https://doi.org/10.1088/1742-6596/379/1/012036
46. Bonan RF, Mota MF, da Costa Farias RM et al (2019) In vitro antimicrobial and anticancer properties of TiO_2 blow-spun nanofibers containing silver nanoparticles. Mater Sci Eng C 104:109876. https://doi.org/10.1016/j.msec.2019.109876
47. Ferraris S, Spriano S, Miola M et al (2018) Surface modification of titanium surfaces through a modified oxide layer and embedded silver nanoparticles: effect of reducing/stabilizing agents on precipitation and properties of the nanoparticles. Surf Coat Technol 344:177–189. https://doi.org/10.1016/j.surfcoat.2018.03.020
48. Hassan ME, Liu G, Omer EOM et al (2018) Silver embedded C-TiO_2 exhibits improved photocatalytic properties with potential application in waste water treatment. Arab J Chem. https://doi.org/10.1016/j.arabjc.2018.12.004
49. Gazzotti S, Rampazzo R, Hakkarainen M et al (2019) Cellulose nanofibrils as reinforcing agents for PLA-based nanocomposites: an in situ approach. Compos Sci Technol 171:94–102. https://doi.org/10.1016/j.compscitech.2018.12.015
50. Zhao SJ, Wang SQ, Ye HQ (2001) Partial reduction of Si(IV) in SiO_2 thin film by deposited metal particles: an XPS study. Surf Interface Anal 32:189–192. https://doi.org/10.1002/sia.1034
51. Bauer AW, Kirby WMM, Sherris JC, Turck M (1966) Antiobiotic susceptibility testing by a standardized single disk method. Am J Clin Pathol 45:493–496
52. Clinical and Laboratory Standards Institute (2012) Performance standards for antimicrobial disk susceptibility tests: approved standard, 11th edn. Clinical and Laboratory Standards Institute, Wayne
53. Yallappa S, Manjanna J, Dhananjaya BL (2015) Phytosynthesis of stable Au, Ag and Au–Ag alloy nanoparticles using J. Sambac leaves extract, and their enhanced antimicrobial activity in presence of organic antimicrobials. Spectrochim Acta Part A Mol Biomol Spectrosc 137:236–243. https://doi.org/10.1016/j.saa.2014.08.030
54. Hajipour MJ, Fromm KM, Akbar Ashkarran A et al (2012) Antibacterial properties of nanoparticles. Trends Biotechnol 30:499–511. https://doi.org/10.1016/j.tibtech.2012.06.004
55. Kanmani P, Rhim JW (2014) Physical, mechanical and antimicrobial properties of gelatin based active nanocomposite films containing AgNPs and nanoclay. Food Hydrocoll 35:644–652. https://doi.org/10.1016/j.foodhyd.2013.08.011
56. Jokar M, Abdul Rahman R, Ibrahim NA et al (2012) Melt production and antimicrobial efficiency of low-density polyethylene (LDPE)-silver nanocomposite film. Food Bioprocess Technol 5:719–728. https://doi.org/10.1007/s11947-010-0329-1
57. De Moura MR, Mattoso LHC, Zucolotto V (2012) Development of cellulose-based bactericidal nanocomposites containing silver nanoparticles and their use as active food packaging. J Food Eng 109:520–524. https://doi.org/10.1016/j.jfoodeng.2011.10.030
58. Dias HB, Bernardi MIB, Bauab TM et al (2019) Titanium dioxide and modified titanium dioxide by silver nanoparticles as an anti biofilm filler content for composite resins. Dent Mater 35:e36–e46. https://doi.org/10.1016/j.dental.2018.11.002

59. Supaphol P, Thanomkiat P, Junkasem J, Dangtungee R (2007) Non-isothermal melt-crystallization and mechanical properties of titanium(IV) oxide nanoparticle-filled isotactic polypropylene. Polym Test 26:20–37. https://doi.org/10.1016/j.polymertesting.2006.07.011
60. Pantani R, Gorrasi G, Vigliotta G et al (2013) PLA-ZnO nanocomposite films: water vapor barrier properties and specific end-use characteristics. Eur Polym J 49:3471–3482. https://doi.org/10.1016/j.eurpolymj.2013.08.005
61. Robertson GL (2013) Food packaging : principles and practice. CRC Press, Boca Raton
62. Ding Q, Shi Y, Chen M et al (2016) Ultrafast dynamics of plasmon–exciton interaction of Ag nanowire-graphene hybrids for surface catalytic reactions. Sci Rep. https://doi.org/10.1038/srep32724
63. Zhao M, Gong H, Ma M et al (2019) A comparative antibacterial activity and cytocompatibility for different top layers of TiN, Ag or TiN–Ag on nanoscale TiN/Ag multilayers. Appl Surf Sci 473:334–342. https://doi.org/10.1016/j.apsusc.2018.12.159
64. Auffan M, Rose J, Bottero JY et al (2009) Towards a definition of inorganic nanoparticles from an environmental, health and safety perspective. Nat Nanotechnol 4:634–641. https://doi.org/10.1038/nnano.2009.242
65. Pérez-Maldonado IN, Herrera C, Batres LE et al (2005) DDT-induced oxidative damage in human blood mononuclear cells. Environ Res 98:177–184. https://doi.org/10.1016/j.envres.2004.11.001

Affiliations

M. G. Peña-Juárez[1] · M. Robles-Martínez[1] · K. B. Méndez-Rodríguez[2] · R. López-Esparza[3] · Elías Pérez[4] · J. A. Gonzalez-Calderon[5]

✉ M. Robles-Martínez
robles.mar@hotmail.com

✉ J. A. Gonzalez-Calderon
amir@ifisica.uaslp.mx

[1] Doctorado Institucional en Ingeniería y Ciencia de Materiales, Universidad Autónoma de San Luis Potosí, Sierra Leona No. 550 Col. Lomas 2da. Sección, 78210 San Luis Potosí, SLP, Mexico

[2] Centro de Investigación Aplicada en Ambiente y Salud, CIACYT, Facultad de Medicina, Universidad Autónoma de San Luis Potosí, Av. Venustiano Carranza 2405, 78290 San Luis Potosí, SLP, Mexico

[3] Departamento de Física, Universidad de Sonora, 1626, 83000 Hermosillo, Sonora, Mexico

[4] Instituto de Física, Universidad Autónoma de San Luis Potosí, Alvaro Obregón 64, 78000 San Luis Potosí, SLP, Mexico

[5] Cátedras CONACYT-Instituto de Física, Universidad Autónoma de San Luis Potosí, Av. Manuel Nava #6, Zona Universitaria, 78290 San Luis Potosí, SLP, Mexico